Self-consistent dynamics of wall slip

Johan L. A. Dubbeldam* and Jaap Molenaar
Faculty of Mathematics and Computer Science, Technische Universiteit Eindhoven, Den Dolech 2, 5600 MB Eindhoven, The Netherlands
(Received 13 August 2002; published 15 January 2003)

A simple molecular model is studied to explain wall slip in a polymer melt. We consider a tube model for tethered chains in which the most important relaxation mechanisms: convective constraint release and chain stretching (retraction), are incorporated. Furthermore, we take the interactions between tethered chains and bulk flow self-consistently into account. Numerical simulations show that our model exhibits an entanglement-disentanglement transition, leading to a jump in the slip velocity which increases with the number of entanglements and the grafting density. The wall shear stress is found to be a nonmonotonic function of the slip and plate velocity, yielding the possibility of hysteresis and spurt instabilities. In a simplified version of the model we show via an analytical approach that the stick-slip transition is asymmetrical: the transition from stick to slip is much faster than the slip to stick transition. Our analysis reveals the existence of a dimensionless parameter that determines the time scale of the dynamics for the slowing down of the bulk flow. The relative rate at which relaxation of the tethered chains and slowing down of the bulk take place, seems to be quintessential for the slip behavior of the melt.

DOI: 10.1103/PhysRevE.67.011803 PACS number(s): 61.25.Hq, 83.10.Mj, 83.10.Kn

I. INTRODUCTION

The so-called no-slip boundary condition has been scrutinized since a long time. Molecular dynamics simulations [1] and experiments have shown that for Newtonian fluids the no-slip condition is in general satisfied. However, for polymer flows (melts) it has been known for many years that slip may occur if a polymer melt flows along a solid surface [2]. In 1979 de Gennes [3] argued that slippage in polymer flows is due to the high viscosity of polymeric fluids. If long polymer chains are grafted on a solid interface, the slip is greatly reduced, but does not disappear [4]. In this case one has a transition from stick to slip boundary conditions. It was realized that the mechanism governing the change from stick to slip boundary conditions could be found in an entanglement-disentanglement transition.

Many investigations of different aspects of this transition have been performed. Some of them used highly complicated models for the polymer flow and most of them consider the slip velocity as given [4–6]. Our goal is to provide a self-consistent physical picture of wall slip for the case in which the slip is caused by disentanglement of chains grafted on the wall from the polymers in the bulk. We will restrict ourselves to polymer melts, for these are of most interest for practical purposes.

The entanglement-disentanglement mechanism, as proposed in Refs. [3,4], predicts that there are essentially three different slip regimes. In the first regime the velocity near the wall is very small, so that the tethered molecules will entangle with the flow and have a more or less random spherical configuration. The friction between the tethered molecules and the melt will be Stokes-like, that is, it is proportional to the radius of gyration of the attached molecule, which depends linearly on the square root of the polymerization index N. In this regime, the wall shear stress increases monotonically with the velocity near the wall, which can be identified with the (wall) slip velocity. When the slip velocity increases beyond a certain value, we enter the second regime in which the tethered molecules no longer have a spherical shape, but are stretched to a degree at which the friction scales linearly with N, so-called Rouse friction. Since this friction force is much weaker than the Stokes friction, the molecule retracts, after which it will stretch again. This motion is called *breathing* and the range of velocities for which this occurs is designated as the *marginal regime*. Breathing implies that the time-averaged stress is constant for a range of velocities. The instantaneous stress is oscillating, reaching a maximum when the tethered and bulk chains are maximally entangled and a minimum when the entanglements are released. When the velocity near the wall increases still more, we reach the third regime in which the tethered molecule is completely disentangled from the melt and almost permanently in a stretched state so that the friction is Rouse-like. In the third regime, the stress near the wall increases again monotonically with the slip velocity.

If instead of the flow velocity near the wall, the shear stress is considered as the independent quantity one finds the following. When the wall shear stress is very small, there will be a negligible slip velocity. This slip velocity increases monotonically with the shear stress, until a critical value of the shear stress is reached. When the stress is increased beyond this value, a large increase in the slip velocity is observed after which the slip velocity will again increase slowly with wall shear stress.

The theory behind the mechanism of slip and some modified versions thereof [4–6] have been experimentally confirmed in Refs. [7–9]. In these papers the wall slip velocity has been directly measured in the vicinity of the wall. It displays a transition from low slip to high slip as a function of the apparent shear rate. However, for grafting densities for which the theory of Ref. [3] should apply, the measured transition is much less steep than predicted [9]. Only for grafting densities more than ten to hundred times higher than the critical grafting density, a steep transition from no slip to slip is observed.

*FAX: +31-40-244-2489. Email address: jdubbeld@win.tue.nl

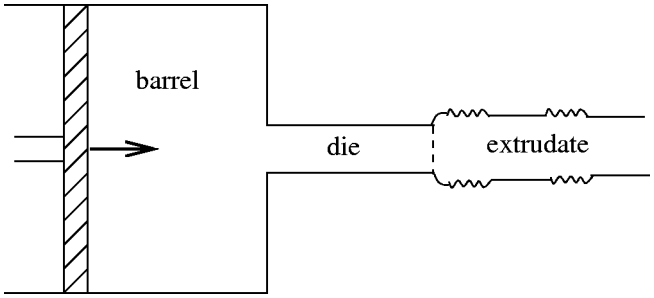

FIG. 1. A sketch of the setup for an extrusion experiment. The pulsating output is due to spurt. The undulations superposed on the pulsations indicate sharkskin.

In most experiments evidence of slip is indirect. In an extrusion experiment as sketched in Fig. 1, the throughput is measured as a function of the pressure difference or vice versa. Increasing the piston speed, which amounts to increasing the wall shear stress, gives rise to (surface) instabilities, such as *sharkskin*, *spurt*, and *gross melt fracture*. The pressure often shows an intermediate regime of large oscillations, usually denoted by spurt. Sharkskin indicates small surface distortions and gross melt fracture is commonly used for large distortions which not merely affect the surface, but also the volume of the extrudate. In Refs. [10,11] it was demonstrated qualitatively that some of these instabilities may originate from a stick-slip phase transition. Their description in terms of Ginzburg-Landau theory requires a nonmonotonic relation between the slip velocity and the wall shear stress, which was simply assumed. Here we show how the slip velocity versus shear stress relation depends on the molecular parameters, and that a nonmonotonic relation between shear stress and slip velocity can actually occur.

Although the entanglement-disentanglement phenomenon gives a good qualitative description of the fact that polymer systems exhibit a nonzero slip velocity at the wall, the time dependent dynamics of the transition is usually not considered. Theories that do describe the dynamics of polymeric fluids are reptation theories in which stresses are calculated for a prescribed shear rate. In stick-slip situations the flow is not constant in time, but changes due to entanglements between tethered and bulk chains, which suggests that one cannot use a prescribed shear rate description. One way to overcome these difficulties is to separate the flow region into two parts: a layer near the wall, the so-called interfacial layer, and a bulk layer which comprises all the polymers which do not belong to the interfacial layer. This method has been pursued in Refs. [12,13], and gives results that agree rather well with experiments.

Here we follow a complementary approach, based on the full dynamics of the grafted chains, which takes the influence of the grafted chains on the bulk flow into account in a self-consistent way. This means that we have to consider both the drag force of the bulk on the grafted chains and the action of the grafted molecules on the flow (velocity) of the polymers in the bulk. For the movement of the grafted chains we need to invoke molecular theories describing entangled polymer systems.

A very successful model for the flow of entangled polymers is a modified version of the Doi Edwards theory that was put forward by Mead, Larson, and Doi [14]. It describes entangled polymers which can reptate, retract, stretch, and show contour length fluctuations. Furthermore, the relaxation mechanism which is crucial for intermediate times in shear flow systems, the so-called convective constraint release (CCR) mechanism, was taken into account. The model was coined contour variable model and consists of a set of partial differential equations for the stress tensor, the contour length, and orientation of the polymers. Very recently this contour variable model has been applied to model wall slip [12]. Since we are interested in the stick-slip transition and the physical mechanism behind it, we concentrate on the dynamics of the grafted chains and their interactions with the bulk. We therefore solve the equations of motion of the grafted chains numerically, which amounts to solving a system of stochastic differential equations.

Recently, this approach of handling polymer flows has also been successfully applied to the single- and double-step strain case [15]. The model presented here is of a similar nature as the one employed in Ref. [15], but adapted to the case of tethered polymer chains in a bulk environment. Furthermore, our description contains all ingredients that were also present in Refs. [12,14], but it additionally provides us with a clear physical picture behind the slip mechanism.

The entanglements between tethered and bulk chains give rise to constraints for the tethered chains. These constraints are depicted as points, which form a grid through which the tethered chain cannot pass. The entangled grafted chain finds its way by performing a random walk, caused by thermal fluctuations and interactions with the bulk molecules. We remark that the rate of entanglement between grafted and nongrafted molecules is determined by two competing mechanisms.

(1) The bulk molecules passing tend to squeeze the grafted chains against the wall. If the chains would not be subject to random forces, the chains would just align with the flow and in their final equilibrium state the molecules would all be maximally stretched and lying along the wall.

(2) Since there are Brownian forces, the chains are continuously changing there conformation, thereby creating new or annihilating existing entanglements with the bulk polymers. These volatile conformational changes are often called contour length fluctuations when the fluctuations are small, or breathing modes, when the tube is really renewed.

Thus, we may summarize as follows. In our model the interactions between the bulk molecules in the flow and the grafted chains are accounted for in a self-consistent way, that is, the velocity profile of the bulk molecules is slowed down due to entanglements between grafted and bulk chains and simultaneously the attached polymer chains are dragged along with the flow. This will lead to a velocity profile in which two regions can be distinguished. In the layer near the wall, the interfacial layer, the velocity rapidly decreases, whereas in the remaining region, the bulk region, the shear rate is constant. A similar division in two layers was also performed in Refs. [12,13], but there the thickness of the boundary layer did not depend on the shear rate, but was

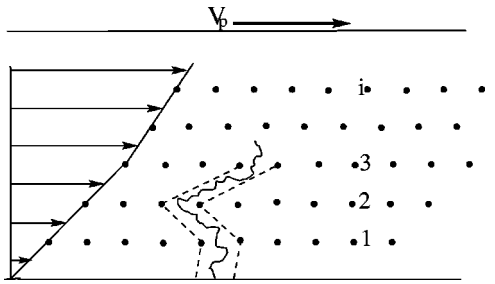

FIG. 2. Sketch of the flow of the grid of constraints. Due to interactions between the grafted chains and the bulk molecules, the velocity is smallest near the wall. In the self-consistent approach not only the interactions of the bulk polymers on the grafted chains are taken into account, but also the reaction of the bulk. The interactions between grafted chains and bulk molecules are local at the entanglement points. This establishes a similar restricted movement of the tethered chain as the depicted tube.

simply a parameter. Here we calculate the thickness of the interfacial layer and the velocity profile within this layer self-consistently, which shows that they depend on the shear rate.

We should further stress that the model does not require the slip velocity to be prescribed. The slip velocity is defined as the velocity of that layer of the bulk polymers near the wall, which is the first layer not entangled with the grafted chains in the interfacial layer. It follows from self-consistent simulations that the slip velocity depends on the upper plate velocity in plane Couette flow and a few molecular parameters. We observe that the velocity exhibits a jump as a function of the plate velocity, which is more pronounced when the polymerization index N of the grafted chains increases or when the distance between entanglements N_e decreases. We also find that the onset of slip increases approximately linearly with the grafting density ν, which has also been predicted in Ref. [5] and confirmed experimentally.

Moreover, the relation between stress and slip velocity is shown to be a nonmonotonic function. An ingredient which, when coupled to the momentum equation for the bulk flow, can for example give rise to the spurt instability [10].

This paper is divided into four sections. In the following section we will give a detailed description of the model. The numerical results are presented in Sec. III and the conclusions and discussion are given in Sec. IV.

II. DESCRIPTION OF THE MODEL

In this paper we study the interaction between chains attached to the wall and flowing bulk chains. Since the interaction takes place in a layer near the wall whose thickness is maximally equal to the radius of gyration (in the limit of no flow), we may choose the situation further away from the wall as simple as possible. That is why we study plane Couette flow. It has the additional advantage that experimental data are available for this case [7–9]. In Fig. 2 a sketch (not on scale) of the velocity profile in the boundary layer is presented. It should be realized that in steady state conditions the flow has a linear velocity profile in the bulk, but not in the interfacial layer near the wall. The velocity profile in this layer is not given beforehand, but is one of the unknowns to be determined in a self-consistent way [16–21].

The grafted chains are supposed to be distributed along the wall with average density ν. The interaction between different grafted chains is neglected, which implies that the grafting concentration is sufficiently low, i.e., $\nu R_0^2 < 1$, where R_0 denotes the radius of gyration of the grafted chains. This situation is often referred to as the mushroom regime. Later on we shall apply the model also for higher grafting densities, since experiments suggest that the interaction between grafted chains can still be neglected, for densities up to more than ten times the critical density $\nu_c = 1/R_0^2$ [9].

Due to its thermal energy or volatility a tethered chain will find its way in the dynamic network of the bulk molecules passing by. Since a grafted chain cannot freely reptate, its motion may be referred to as breathing, like in star-shaped polymers [24]. The grafted chains stretch and contract in a breathing fashion, the motion just being restricted by the constraints imposed by the bulk molecules and the wall. These constraints make the movement of the grafted chain predominantly take place in a tubelike region [22], of which one end is constantly destroyed and recreated in an entanglement-disentanglement process, such that after some time an entirely new tube is formed [23].

To study the dynamics of the entanglement-disentanglement process, we need to represent the bulk molecules such that simulations can be done in a reasonable time span. To that end we introduce the following model. The flowing bulk molecules, which act as potential entanglement points for the tethered chains, are represented by obstacles on a lattice. To reduce the model to its essentials, we assume that the breathing motion of a tethered chain is restricted to two-dimensional motion taking place in the plane perpendicular to the wall and parallel to the flow direction. The situation is sketched is Fig. 2. Initially the grid of obstacles in this plane is square with lattice parameter a. The grid points move parallel to the wall. Grid points in the same horizontal layer have equal velocities, so that they keep a constant distance a. It is important to realize that the velocities of the layers are different and have to be calculated.

The interaction between the grid and the grafted chains takes place at localized points where the grid points and the grafted chains touch; these points are called entanglements. Since the number of entanglements increases when the distance to the wall decreases, the velocity is rapidly decreasing in the vicinity of the wall.

When the obstacles are moving parallel to the wall, they drag the tethered chains that are entangled with one or more layers along. If a tethered chain is entangled with a layer, it will slow down the layer's velocity, since there is mutual interaction between the bulk layers and grafted chains, that is, the grafted chains stretch and the bulk layers slow down. As the chains stretch, stress is built up in the chain, which is only relaxed when the chain retreats from the layer and loses contact with it. One reason for losing entanglements is that the constraints are simply convected away. This process is referred to as CCR. If the tethered chains would be passive ropes, this would eventually result in a rope configuration

without any entanglements between bulk and grafted molecules. This amounts to a configuration in which the rope is squeezed against the wall. In this case the interaction between the bulk and attached chains is only by (Rouse) friction, which is much smaller than the entanglement interaction. The passive rope scenario sketched above is in practice counteracted by the volatility of the grafted chains.

In our model we describe the grafted chains by bead-spring or so-called Rouse chains. If such a grafted chain gets entangled with one or more moving layers, stress is induced in the chain. Several stress relaxation mechanisms now become relevant. On short time scales the beads are redistributed, such that the induced stress is equally distributed among the tube segments. The length fluctuations of chains occur on the same time scale (Rouse time).

Reorientation of the chains happens on a much longer time scale. This can occur by the breathing process described above, CCR, or simply constraint release (CR). Constraint release is the process that is due to reptation of the bulk chains: the constraints on the tethered chain disappear, which can therefore relax [6]. This process is particularly important when the environment consists of chains that are relatively short. Since the length of a grafted chain is usually considerably shorter than the length of the bulk chains, due to the fact that a single grafted chain may be in contact with the wall at several places, this relaxation process can be neglected in our considerations. In the model presented below the most relaxation mechanisms for grafted chains, breathing, and CCR, are accounted for. The slip law we are aiming at is mostly determined by the competition between CCR and breathing relaxation mechanisms.

After this general description of the model we will now focus on the evolution equations for the grafted chains.

A. Dynamics of the tethered chains

We consider a chain attached to the wall consisting of N beads and connected by $N-1$ springs. With exception of the first and last beads, and the beads adjacent to an entanglement, they satisfy the Langevin equation

$$\zeta_1 \frac{\partial \mathbf{x}_n}{\partial t} = k[\mathbf{x}_{n+1}(t) + \mathbf{x}_{n-1}(t) - 2\mathbf{x}_n(t)] + \mathbf{f}_n(t), \qquad n = 2, \ldots, N-1, \quad (1)$$

where ζ_1 is the friction coefficient of a monomer, $\mathbf{x}_n(t)$ describes the position of the nth bead. In view of the fluctuation-dissipation theorem the spring constant k is related to the temperature T by

$$k = \frac{3k_B T}{b^2}. \quad (2)$$

Here b denotes the Kuhn length and $\mathbf{f}_n(t)$ is the Brownian force, whose components $f_n^i(t)$ satisfy

$$\langle f_n^i(t) \rangle = 0, \quad \langle f_n^i(t_1) f_m^j(t_2) \rangle = 2k_B T \zeta_1 \delta(t_1 - t_2)\, \delta_{nm} \delta_{ij},$$

where i,j stand for x or y.

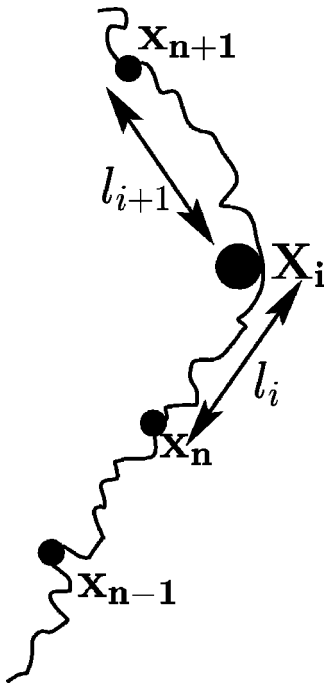

FIG. 3. Detail of the chain conformation. The obstacle at $\mathbf{X}_i$ indicated by the large circle interacts with the beads at $\mathbf{x}_n$ and $\mathbf{x}_{n+1}$ by streching the spring that connects them. At the same time the velocity of the obstacle is reduced due to the increased tension in the spring which is exerting a reaction force on the obstacle.

The first bead is attached to the wall at $\mathbf{x}_1 = (x_1, 0)$. Modification of Eq. (1) for the first and last beads is straightforward. Equation (1) only applies when the chain has no interaction with a layer. In the vicinity of an entanglement the chain is dragged along with the bulk flow by the obstacles. This interaction with a layer is highly local. The influence of the entanglement is felt by the rest of the chain indirectly, namely, through their interactions with the neighboring beads. This implies that Eq. (1) is only valid for the beads not adjacent to an obstacle. These beads satisfy an adjusted equation. In Fig. 3, we show a detail of the situation in which a grid point with coordinate vector $\mathbf{X}_i$ hits the chain between two beads with coordinates $\mathbf{x}_n$ and $\mathbf{x}_{n+1}$. The force exerted on this bead by the spring between $\mathbf{x}_n$ and $\mathbf{x}_{n-1}$ is simply given by $k(\mathbf{x}_{n-1} - \mathbf{x}_n)$.

The force stemming from the interaction between the nth and $(n+1)$th bead is mediated by the spring, which is bent along an obstacle $\mathbf{X}_i$, and it is given by $k(l_i + l_{i+1})$. So, the force is proportional to the total length of the spring which consists of two parts l_i and l_{i+1} as is indicated in Fig. 3. The force between the nth and $(n+1)$th bead points in the direction of $\mathbf{X}_i - \mathbf{x}_n$. The total force $\mathbf{F}_n$ felt by the nth bead reads as

$$\mathbf{F}_n = k(\mathbf{x}_{n-1} - \mathbf{x}_n) + k(l_i + l_{i+1}) \frac{\mathbf{X}_i - \mathbf{x}_n}{l_i}. \quad (3)$$

For the force on bead $(n+1)$ we similarly find

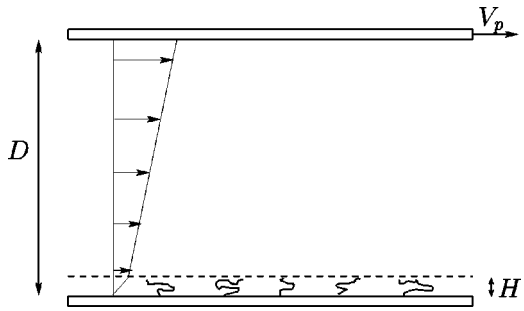

FIG. 4. Schematic representation of plane Couette flow. There are two different regions, the interfacial layer and the bulk layers. The thickness of the interfacial layer H depends on the plate velocity V_p, and is largest (of the order of the gyration radius), when the upper plate is not moving at all, so when $V_p=0$.

$$\mathbf{F}_{n+1}=k(\mathbf{x}_{n+2}-\mathbf{x}_{n+1})+k(l_i+l_{i+1})\frac{\mathbf{X}_i-\mathbf{x}_{n+1}}{l_{i+1}}. \tag{4}$$

Beads adjacent to an entanglement obey evolution equation (1) with the term proportional to k replaced by $\mathbf{F}_n$ or $\mathbf{F}_{n+1}$ depending on the position of the bead relative to the entanglement point.

If we nondimensionalize our equations and use as unit of length the Kuhn length b and as unit of time τ defined by

$$\tau=\frac{b^2\zeta_1}{3k_BT}, \tag{5}$$

we can recast Eq. (1) into the form

$$\frac{\partial\overline{\mathbf{x}}_n}{\partial\overline{t}}=\overline{\mathbf{x}}_{n+1}+\overline{\mathbf{x}}_{n-1}-2\overline{\mathbf{x}}_n+\mathbf{G}_n(\overline{t}), \tag{6}$$

where

$$\overline{\mathbf{x}}=\frac{\mathbf{x}}{b}, \quad \overline{t}=\frac{t}{\tau}, \tag{7}$$

are dimensionless quantities. Note that $\tau=\tau_R\pi/N^2$, where τ_R is the Rouse relaxation time of the chain. The choice of τ as unit of time leads to equations with a very convenient form. The components of the dimensionless random forces $G_n^i(\overline{t})$ now satisfy

$$\langle G_n^i(\overline{t})\rangle=0, \quad \langle G_n^i(\overline{t}_1)G_m^j(\overline{t}_2)\rangle=\frac{2}{3}\delta(\overline{t}_1-\overline{t}_2)\delta_{mn}\delta_{ij}.$$

The nondimensionalization of the equations for the beads adjacent to an entanglement point which contain $\mathbf{F}_n$ or $\mathbf{F}_{n+1}$ is analogous. Having obtained the evolution equations of the tethered chains we now turn to their influence on the velocity of the chains in the polymer bulk.

B. Dynamics of the bulk chains

We derive the equation of motion for the grid layers. We assume the flow to be described as a system which consists of P layers moving in parallel. This is also depicted in Figs. 2 and 4. Layer P is farthest away from the lower wall and its velocity is prescribed. The velocity profile, i.e., the layer velocities $v_i, i=1,\ldots,P-1$, are obtained from the simulations. Let us first consider a situation without chains grafted on the wall. The interaction between two neighboring layers takes place via molecular friction mostly due to entanglements. Its strength is measured by the viscosity η. In this paper we take η constant, but shear thinning via a shear dependent viscosity can easily be incorporated in the simulations. The dimensionful equation of motion for layers $i=2,\ldots,P-1$ is

$$\rho a\frac{dv_i}{dt}=-\eta(2v_i-v_{i+1}-v_{i-1}), \tag{8}$$

where a is the distance between two layers and ρ is the mass density of the melt. The first layer has to be treated separately, since it interacts via (Rouse) friction with the wall [4,9]. For layer one we have

$$\rho a\frac{dv_1}{dt}=\eta(v_2-v_1)-F_W(v_1). \tag{9}$$

The friction force F_W depends on v_1 and the material properties. As F_W is monotonically increasing, the system given by Eqs. (8) and (9) has a unique steady state that is linear in the distance i from the wall. The system converges to the steady state with a factor approximately given by $\exp(-\eta/\rho a)$. A special case is the so-called plug flow, where $F_W=0$, with steady state $v_i=v_P, i=1,\ldots,P-1$. Another extreme case is obtained when F_W is much larger than the shear forces. In this case $v_1=0$ and $v_i=(i-1/P-1)v_P$ for $i>1$.

The next modeling step is the representation of one or more layers interacting with a grafted chain. The chain is attached to the wall at $\mathbf{X}_0$, say. The chain will create its first entanglement with layer 1 at entanglement point $\mathbf{X}_1$. Its second entanglement at position $\mathbf{X}_2$ is probably with layer 2, but it might also happen that the chain crosses layer 1 again from above. The next entanglement point $\mathbf{X}_3$ is situated in one of the layers 1, 2, or 3. So, if a grafted chain has M entanglements, its conformation or tube is characterized by $\mathbf{X}_i, i=1,\ldots,M$, entanglement points, which lie scattered over the grid layers near the wall. Given the $\mathbf{X}_j$, the dynamics of the chain, that is, of all its constituting beads are governed by the equations of motion given in Sec II A. Rearrangement of the beads during a time step in the calculation may cause the creation of an extra entanglement $\mathbf{X}_{M+1}$ or annihilation of the last entanglement $\mathbf{X}_M$.

If two entanglements $\mathbf{X}_j$ and $\mathbf{X}_{j+1}$ are in neighboring layers, these layers have interaction via the part of the grafted chain between $\mathbf{X}_j$ and $\mathbf{X}_{j+1}$. This part forms a linear spring between $\mathbf{X}_j$ and $\mathbf{X}_{j+1}$ with spring constant k_j and therefore the expression for k_j which is valid for a Rouse chain in a tube [22] applies

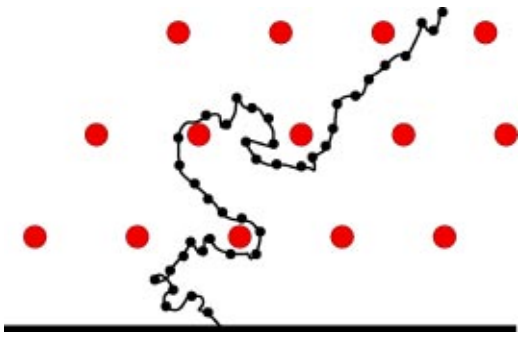

FIG. 5. Picture of a tethered chain which has interaction with four grid points. One of the more intricate configurations that can occur during the simulation process: the chain passes through the second layer into the third layer and subsequently enters the second layer again from the above.

$$k_j = \frac{3k_B T}{N_j b^2}, \tag{10}$$

where N_j is the number of beads between $\mathbf{X}_j$ and $\mathbf{X}_{j+1}$. From the literature [22,24] we know that $a = \sqrt{N_e} b$, where N_e is the average value of N_j for a chain in equilibrium. The parameters b and N_e depend on the type and density of the polymer and are known for many systems. The bookkeeping of the entanglements $\mathbf{X}_j$ is important in our calculations. The effect of neighboring layers being connected by parts of a grafted chain is most easily explained if we consider a grafted chain for which the distance of $\mathbf{X}_j$ from the wall increases monotonically with i. If $\mathbf{X}_j = (X_j, Y_j)$ then $Y_j = ja$ in this special case and the equation of motion of the layer $j, j = 2, \ldots, M-1$, is

$$\rho a \frac{dv_j}{dt} = -\eta(2v_j - v_{j+1} - v_{j-1}) + k_j(X_{j+1} - X_j) - k_{j-1}(X_j - X_{j-1}). \tag{11}$$

For layer M, which is farthest away from the wall, we have

$$\rho a \frac{dv_M}{dt} = -\eta(2v_M - v_{M+1} - v_{M-1}) - k_M(X_M - X_{M-1}) \tag{12}$$

and for the first layer

$$\rho a \frac{dv_1}{dt} = -\eta(v_1 - v_2) + k_2(X_2 - X_1) - k_1(X_1 - X_0) - F_W(v_1). \tag{13}$$

We emphasize that in reality the bookkeeping is much more intricate. Figure 5 shows that it may happen that two neighboring layers are connected by two different parts of the same grafted chain. To elucidate the basic principles of the present model we show how it works in an extremely simple situation.

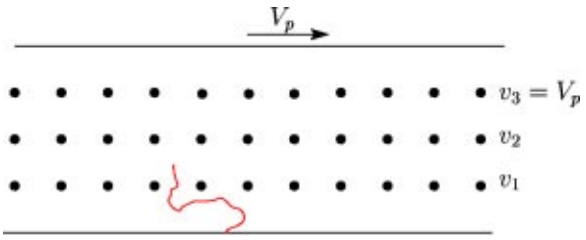

FIG. 6. Sketch of the three layered system. The plate velocity V_p is transmitted entirely to the third layer and there is only one entanglement, between the grafted chains and the first layer of the bulk molecules.

Stick-slip transition in a system with three layers

In this subsection we make some simplifying assumptions in order to obtain an analytical estimate for one of the typical time scales in the problem. It is not supposed to explain the numerical simulations of the full system which will be discussed later.

We consider the configuration with three grid layers as sketched in Fig. 6. The third layer has a prescribed velocity v_3 equal to the plate velocity V_p. Moreover, in this example there is a permanent entanglement $\mathbf{X}_1$ with layer 1. We assume that the particular chain we consider represents ν chains per unit area grafted on the wall of which ν_1 have an entanglement with layer 1. In this particular example, in which all chains are assumed to be entangled with the first layer, we have $\nu = \nu_1$. If not all grafted chains would interact with the first layer, $\nu_1 < \nu$, and $\nu - \nu_1$ tethered chains per unit area would be squeezed against the wall. In reality ν_1 will be, after time averaging, a function of V_p and an outcome of the simulations. For simplicity, we take ν_1 here to be known in advance and constant.

The dimensionful equations for the velocities v_1 and v_2 for layers one and two are

$$\rho a \frac{dv_1}{dt} = \eta(v_2 - v_1) - k_1 \nu_1 (X_1 - X_0) - F_W(v_1),$$
$$\rho a \frac{dv_2}{dt} = \eta(v_3 + v_1 - 2v_2). \tag{14}$$

The first equation shows that the velocity of the first layer is enhanced as a consequence of viscous friction between the first and second layer and is reduced due to entanglements with the grafted chain and friction with the wall F_W. The second equation expresses that layer 2 experiences viscous friction from its two neighboring layers. In the steady state, the velocity v_2 of layer 2 will be equal to the average of v_1 and v_3.

Taking $F_W = 0$ for simplicity, the dimensionless velocities $\bar{v}_1(t)$ and $\bar{v}_2(t)$ satisfy

$$\frac{d\bar{v}_1}{d\bar{t}} = \frac{\eta\tau}{\rho a^2}(\bar{v}_2 - \bar{v}_1) - \frac{k_1 \tau^2 \nu_1}{\rho a} \bar{X}_1,$$
$$\frac{d\bar{v}_2}{d\bar{t}} = \frac{\eta\tau}{\rho a^2}(\bar{v}_3 + \bar{v}_1 - 2\bar{v}_2). \tag{15}$$

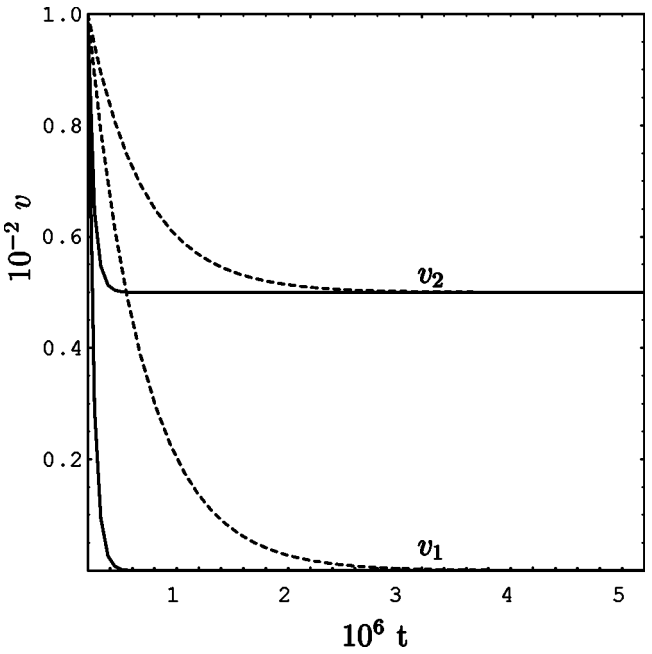

FIG. 7. The evolution of (dimensionless) velocities v_1 and v_2 for two different values of $\epsilon\theta$ plotted as a function of (dimensionless) time t. For the dashed curves $\epsilon\theta=10^{-4}$ and the solid curves represent the case $\epsilon\theta=10^{-6}$. In both cases $V_p=0.01$.

This system of differential equations can be recast into a simple form by introducing the dimensionless parameters $\epsilon=\rho N_e b^2/\eta\tau$ and $\theta_1=3k_BT\tau^2\nu_1/\rho N_e^{3/2}b^3$. Dropping the bars and denoting differentiation with respect to $\bar{t}$ by a dot yields

$$\epsilon\dot{v}_1=v_2-v_1-\theta_1\epsilon X_1,$$

$$\epsilon\dot{v}_2=V_p+v_1-2v_2. \tag{16}$$

The entanglement-disentanglement transition turns out to be a matter of scales. The parameter ϵ is very small, typically of the order of $10^{-11}-10^{-12}$, whereas θ_1 is of order 10^4-10^5, at an entanglement density ν_1 equal to the critical grafting density $\nu_c=(1/R_0^2)(1/Nb^2)$. This implies that Eqs. (16) represent a singularly perturbed system. Since Eqs. (16) are linear, the system can be explicitly solved as is done in the Appendix. Here we will make some qualitative remarks about the system defined by Eqs. (16) and graphically present the solution.

There are two extreme cases. In the first case all the grafted chains reach the first layer, so $\theta_1=\theta_{\max}$, or equivalently $\nu_1=\nu$. In the other extreme case there are no entanglements with the obstacles in the first layer, so ν_1 and therefore θ_1 vanishes. This leads again to the linear velocity profile, as discussed before.

If, for illustrative purposes, θ_1 in Eq. (16) is taken constant in time and equal to $\theta_{\max}$, we find that the velocity in the first and second layer is decreasing with a typical relaxation time τ_c. The solution is shown in Fig. 7 and shows that v_2 approaches the average of v_1 and V_p, which is just $V_p/2$, since v_1 goes to zero and $v_3=V_p$ for all times. The relaxation time τ_c is given by

$$\tau_c=\frac{1}{2\theta_1\epsilon}=\frac{\eta_0 a}{6k_BT\tau_1\nu}=\frac{\eta_0\sqrt{N_e}}{2b\zeta_1\nu}. \tag{17}$$

The time-scale τ_c at which the velocity of the layers in the bulk slows down is a long time scale, due to the smallness of $\epsilon\theta_1$. It is also shown in the Appendix, that when the entanglement is released, the plug flow situation is reestablished almost immediately, and the entire process repeats itself from the beginning. This artificial example clearly shows that in a stick-slip situation the transition from stick to slip is much faster—almost instantaneous—than the transition from slip to stick, which occurs on the time-scale τ_c. Numerical simulations suggest that these two time scales are also present in the full system, and crucial for the occurence of a stick-slip transition.

III. SIMULATION RESULTS

Our aim is to find out how the slip velocity depends on V_p. The slip velocity is defined here as the average speed of the layer closest to the wall that never has entanglements with grafted chains. We performed numerical simulations by integrating the model equations supplemented with suitable boundary conditions. For convenience we took the spring constant k_j, given by expression (10), equal to its equilibrium value $3k_BT/N_eb^2$. This amounts to averaging the force exerted on the bulk layer over the equilibration time, which is reasonable since the entanglements generally persist much longer than the equilibration time of the chain segments [22].

Where possible, the parameter values were taken in accordance with Ref. [9], in which experiments performed on a polydimethylsiloxane (PDMS) melt are described. We consider a configuration in which the distance D between the two plates is 10 μm. The typical length of a Kuhn segment is $b=10$ Å. Furthermore, we take the number of monomers N of a chain attached to the wall fixed and equal to 100 in order to be able to do calculations within a reasonable time span. The average entanglement length N_e is set equal to 10 or 5 in our simulations, which fixes the layer distance since $a=\sqrt{N_e}b$. The temperature T is of the order of 300 K, which implies a time τ of the order of μs, which is in agreement with Ref. [25]. The parameter $\theta_{\max}\epsilon$ will be varied between 10^{-4} and 10^{-7} which corresponds to changing the grafting density from $\nu=0.1\nu_c$ to 100 times the critical density ν_c.

In Fig. 8, a logarithmic plot of the dimensionless slip velocity $\bar{V}_s$ is presented as a function of the (dimensionless) plate velocity $\bar{V}_p$. It displays the three slip velocity regimes that were expected. For small $\bar{V}_p$ the slope of the curve is constant. The value of $\bar{V}_p$ for which the slope starts to increase is denoted by $\bar{V}_p^\star$. For $\bar{V}_p>\bar{V}_p^\star$ the slope has initially a higher value. This region is referred to as the transition region. For very large values of $\bar{V}_p$ the slope approaches one. The transition is only mild and not very sharp in contrast with the predictions in Ref. [3]. From experiments it is

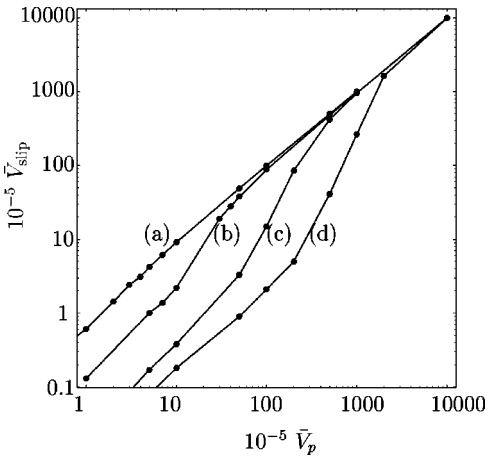

FIG. 8. Plot of the slip velocity as a function of the upper plate velocity $\overline{V}_p$ for $\epsilon\theta_{\max}=10^{-7}$ (a), $\epsilon\theta_{\max}=10^{-6}$ (b), $\epsilon\theta_{\max}=10^{-5}$ (c), and $\epsilon\theta_{\max}=10^{-4}$ (d). The beginning of the transition region increases with increasing $\epsilon\theta_{\max}$ in agreement with experiment and the predictions in Ref. [3]. Also the transition is more pronounced for larger values of $\epsilon\theta_{\max}$, which has also been observed experimentally.

known [9] that the transition depends on the density of the grafted chains and the number of entanglements. In fact, for densities $\nu\approx\nu_c$, no sharp transition is observed experimentally, but only a mild transition comparable to ours [9]. Only when the densities are increased well beyond ν_c, say 10 to 100 times ν_c, the transition is very sharp, almost vertical.

The data of Fig. 8 can also be presented by looking at the so-called extrapolation length l, defined by $l=V_sD/(V_p-V_s)$. We see from Fig. 9, that the l/D versus $\overline{V}_{\rm slip}$ curve exhibits a crossover from a practically constant to an approximately linearly increasing regime. The crossover in the velocity and l/D was also observed in the experiments in

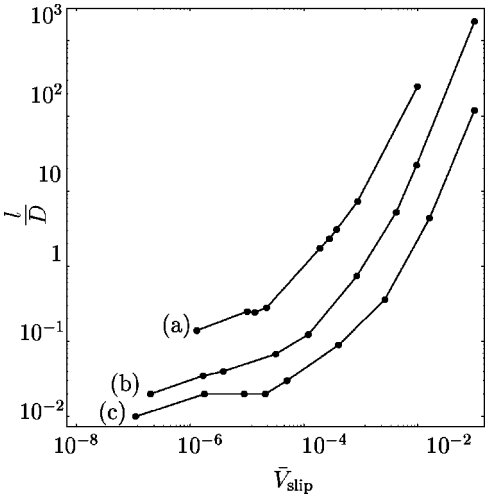

FIG. 9. The extrapolation length l/D as a function of the slip velocity $\overline{V}_{\rm slip}$ for three different values of $\epsilon\theta_{\max}$. Curve (a) corresponds to $\epsilon\theta_{\max}=10^{-6}$, (b) to $\epsilon\theta_{\max}=10^{-5}$, and (c) to $\epsilon\theta_{\max}=10^{-4}$. The sudden increase of $\overline{V}_{\rm slip}$ is most clearly present for $\epsilon\theta_{\max}=10^{-4}$, which has the largest grafting density.

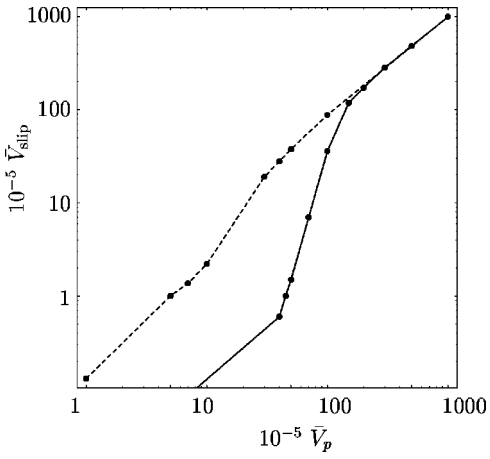

FIG. 10. The slip velocity shown as a function of the upper plate velocity $\overline{V}_p$ for fixed $\epsilon\theta_{\max}=10^{-6}$, but for different values of N_e. The dashed curve corresponds to $N_e=10$ and the solid one to $N_e=5$. The transition for $N_e=5$ clearly is much steeper than for $N_e=10$.

Refs. [7] and [9] and were predicted qualitatively by de Gennes in Ref. [3].

To find the dependence on the number of entanglements we changed the value of N_e to $N_e=5$, which corresponds to enhancing the number of entanglements. The numerical results in this case, together with the $N_e=10$ result for comparison, are depicted in Fig. 10. It shows that the transition becomes sharper with decreasing N_e values. From the simulations it can be inferred that at $\overline{V}_p=\overline{V}_p^{\star}$ the relaxation mechanism for the tethered chains has changed. In fact, $\overline{V}_p^{\star}$ designates the value of the plate velocity above which CCR is the dominating relaxation mechanism of the tethered chains. For plate velocities smaller than $\overline{V}_p^{\star}$, the bulk flow is slowed down so much that the constraints are no longer removed from the tethered chain by CCR, and therefore the other relaxation mechanism, arm retraction, becomes dominant.

Considering the grafted chain conformations and the velocity profile of the grid elucidates the processes that take place if one increases the plate velocity. In Fig. 11 two chain conformations and two velocity profiles are depicted for two different values of $\overline{V}_p$. Chain (a) corresponds to $\overline{V}_p=0.005$ and (b) to $\overline{V}_p=0.001$. Since the bulk flow tries to drag the grafted chains along, there will always be a part of the chain near $\mathbf{X}_0$ that is squeezed between the wall and the first layer. This part of the chain will be longer for higher $\overline{V}_p$, which agrees with Fig. 11. The tail of the chain can escape the dragging of the grid by arm retraction and subsequently tube renewal or breathing. Precisely this process is displayed in Fig. 11. Since the drag is stronger for higher values of $\overline{V}_p$, chain (a) has a smaller tail which point upwards than chain (b). The consequences for the velocity profile are that there is less slowing down for chain (a) than for chain (b), since there are fewer entanglements for (a) than for (b). Also the velocity profile for (b) shows that the velocity decreases faster closer to the wall.

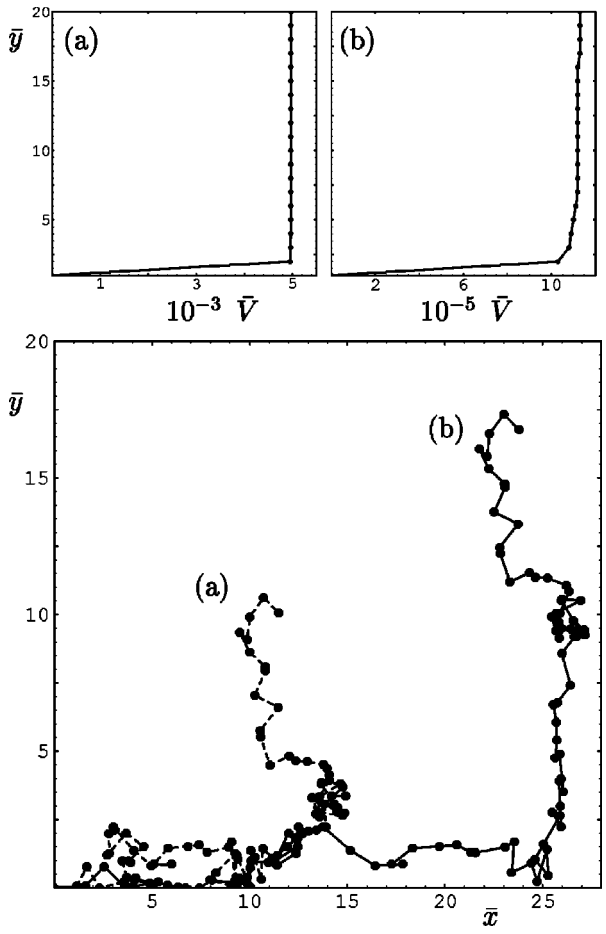

FIG. 11. Two chain conformations and velocity profiles for two different values of $\overline{V}_p$ and fixed values for $\epsilon\theta_{\max}=10^{-6}$ and $N_e=5$. Configuration (a) corresponds to $\overline{V}_p=0.005$ and (b) represents $\overline{V}_p=0.001$. The chains both have a part which is approximately horizontal and a tail that is entangled with the bulk which points upwards. The velocity profile (a) corresponds nearly to plug flow, since the interfacial layer is very small. The velocity profile (b) reveals that the velocity tends to zero over an interfacial layer consisting of a few bulk layers.

Another important quantity is the wall shear stress. It can be calculated by employing the Kirkwood expression to calculate the stress in the chains attached to the wall [22]:

$$\sigma_{xy}^{\text{entang}}(t)=\frac{3ck_BT}{Nb^2}\left\langle \int_0^L dsL(t)u_x(s,t)u_y(s,t)\right\rangle, \quad (18)$$

where c is the number of polymers per unit volume, L the length of the tube and $u_x(s,t),u_y(s,t)$ denote the x and y components of the vector tangent at the tube at position s at time t. The contour length coordinate s is zero at the wall and L at the end of the chain. There is another contribution to the stress besides that given in Eq. (18). At high plate velocities the grafted chains are dragged along with the flow and orient parallel to the wall. Nevertheless, they experience friction due to the bulk chains that flow along, although there are no entanglements. Under entanglement conditions, the latter stress contribution is negligible compared to the stress associated with the entanglements. However, when there are hardly any entanglements left, due to the high plate velocities, the contribution from the friction between the first bulk layer and horizontally oriented grafted chain, called Rouse-friction, is dominant. From physical arguments it is easily seen that the stress σ^{Rouse} corresponding to Rouse friction is given by Ref. [9]

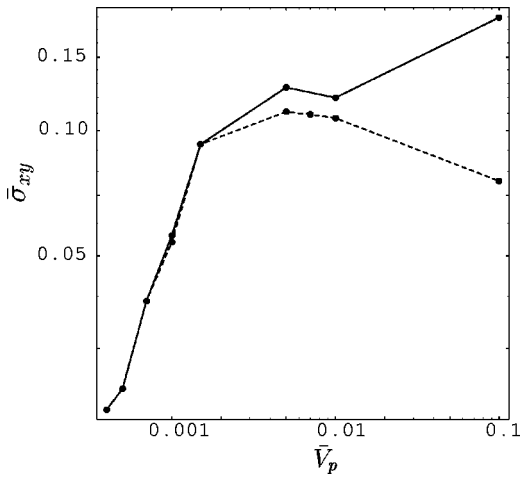

FIG. 12. The dimensionless stress is shown as a function of the plate velocity $\overline{V}_p$. It clearly shows that it attains a maximal value for $\overline{V}_p=0.005$, which is well beyond the value of $\overline{V}_p$ at the onset of slip $\overline{V}_p^{\star}=0.0005$. The dashed line represents the stress contribution due to the entanglements, the solid line is the total stress which includes the Rouse friction part, which becomes dominant when $\overline{V}_p$ is large.

$$\sigma_{xy}^{\text{Rouse}}=\zeta\nu\frac{N}{N_e}V_{\text{slip}}. \quad (19)$$

Here ζ is taken equal to the monomer friction ζ_1 if one assumes that the interaction between the wall and the monomers is equally strong. If this is not the case in practice one needs an expression for ζ which takes into account the characteristics of the wall. Since here we focus on the entanglement-disentanglement transition, we will simply take $\zeta=\zeta_1$. If we add the two stress contributions, we obtain that the total shear stress σ_{xy}^{tot} which is

$$\sigma_{xy}^{\text{tot}}=\frac{3ck_BT}{Nb^2}\left\langle \int_0^L dsL(t)u_x(s,t)u_y(s,t)\right\rangle+\zeta_1\frac{N}{N_e}V_{\text{slip}}. \quad (20)$$

When the chain is aligned with the wall, the first term vanishes and we are left with a term increasing linearly with V_{slip}. The expression we used for the stress is similar to that used in Refs. [12,13]. In Ref. [3] the wall shear stress apart from the Rouse contribution was simply taken to be proportional to the length of the tethered chain. We find that both definitions lead to the same curve, with a maximum for the same value of $\overline{V}_P$.

In Fig. 12 the dimensionless wall shear stress $\overline{\sigma}_{xy}^{tot}$, defined as $\overline{\sigma}_{xy}^{tot}=\sigma_{xy}^{b}/3k_BT\nu_c$, is shown for $N_e=5$. There is a

maximum at $\overline{V}_p = 0.005$, whereas the transition region starts at $\overline{V}_p = \overline{V}_p^\star = 0.0005$. The fact that the maximum in the stress is attained at values of $\overline{V}_p \gg \overline{V}_p^\star$ can be explained as follows. When $\overline{V}_p$ is gradually increased, the stress increases, since the tethered chains will start to orientate in the flow. Increasing the plate velocity beyond $V_p^\star$, does not really change this. The molecule is stretched, but still feels the constraints and therefore the stress continues to increase with $\overline{V}_p$. When $\overline{V}_p$ is sufficiently large to push the tethered chain parallel to the wall, the stress due to entanglements starts to decrease steeply. At the same time the Rouse stress begins to grow linearly with $\overline{V}_p$. This results in the *S*-shaped stress versus plate velocity curve depicted in Fig. 12. From Fig. 8 it follows immediately that plotting the stress as function of the slip velcity would lead to a similar *S*-shaped curve.

IV. CONCLUSIONS AND DISCUSSION

We proposed a self-consistent model to explain wall slip from a molecular point of view. The model contains two important relaxation mechanisms for grafted chains: CCR and arm retraction. It was demonstrated that when the model was evaluated via numerical simulations in a plane Couette-flow geometry for low to moderate grafting densities, it exhibits a stick-slip transition, in agreement with experiments. This can be explained as a transition from arm retraction to CCR as the dominating relaxation mechanism for the tethered chains. The velocity profile was also calculated and shown to be nonlinear in the interfacial layer, where entanglement-disentanglement takes place.

The stress reaches a maximum as a function of the upper plate velocity. The maximum is attained at a value of $\overline{V}_p$ which does not coincide with $\overline{V}_p^\star$, but is much larger. This is due to the fact that only for very large plate velocities the bulk chains succeed in pushing the tethered chains parallel to the wall. If this happens the stress in the tethered chains squeezed against the wall increases linearly with the slip velocity of the bulk molecules sliding along. The resulting wall shear stress versus slip velocity is *S* shaped. Such a nonmonotonic slip wall may give rise to unstable behavior. In Refs. [11,16,26] it was shown that the so-called spurt instability is perfectly described by such a slip law. However, the law used there was introduced heuristically. The approach that was taken here makes it possible to calculate the slip law starting from molecular data. This is essential for any spurt model to have predictive power.

The model developed here contains assumptions which are to be relaxed in future work. In order for our model to be applicable in practice it is necessary to deal with polydispersity. This implies that one has to average over a distribution of chains lengths. If the numerics can be improved upon it is, in principle, feasible to perform numerical simulations for different chain lengths and to obtain the slip velocity and stress as averages of these simulations.

We should also remark that the effect of loops is neglected. This can be justified, since it is far harder for a loop to relax completely and therefore they do not contribute to jumps in the velocity, but rather give an overall slowing down of velocity of the fluid. Such an effect could also be incorporated by putting it into the effective relaxation time of the tethered chains.

The model we considered is only two dimensional. Extension to three dimensions is another refinement, which we would like to include. This would probably have an effect on the simulations, but it is not expected to lead to any qualitatively different results, since the underlying entanglement mechanism remains the same.

So far, we were only able to numerically integrate the evolution equations of the dynamical stochastic system. We are currently investigating analytical aproximations, which would allow us to deduce how the important quantities, such as the beginning of the transition region and the velocity at which the stress maximum is attained, depend on the molecular parameters.

Furthermore, it is well known that the life time of a grafted chain is not infinite, since they debond from the solid surface or break. In fact, the population of the tethered chains not constant, but a dynamical quantity: chains attach and detach continuously. It is a challenge to combine this bonding (debonding) process with the present approach, since then a rather complete picture becomes available allowing for accurate calculation of slip laws for any polymer melt.

ACKNOWLEDGMENTS

This research was performed as a part of the 3PI project Grant No. (G5RD-CT-2000-00238), which is supported by the European Union.

APPENDIX

One can rewrite Eqs. (16) after another differentiation in the matrix form

$$\begin{pmatrix} \dot{x} \\ \dot{y} \\ \dot{z} \end{pmatrix} = \begin{pmatrix} 0 & 1 & 0 \\ 0 & 0 & 1 \\ -\dfrac{2\theta}{\epsilon} & \dfrac{-1-\theta\epsilon^2}{\epsilon^2} & -\dfrac{3}{\epsilon} \end{pmatrix} \begin{pmatrix} x \\ y \\ z \end{pmatrix},$$

where x,y,z now stand for $v_1, \dot{v}_1, \ddot{v}_1$, respectively. The corresponding eigenvalue equation reads as

$$\lambda^3 + \frac{3\lambda^2}{\epsilon} + \lambda\left[\frac{1+\theta\epsilon^2}{\epsilon^2}\right] + \frac{2\theta}{\epsilon} = 0, \tag{A1}$$

where we have written for simplicity θ for θ_1. This third order equation is easily solved and yields the following three negative eigenvalues:

$$\lambda_1 = -\frac{1}{\epsilon}\left[1 + 2\sqrt{\frac{2-\theta\epsilon^2}{3}}\cos\left(\frac{\phi}{3}\right)\right], \tag{A2}$$

$$\lambda_2 = -\frac{1}{\epsilon}\left[1 + 2\sqrt{\frac{2-\theta\epsilon^2}{3}}\cos\left(\frac{\phi}{3} + \frac{2\pi}{3}\right)\right],$$

$$\lambda_3 = -\frac{1}{\epsilon}\left[1+2\sqrt{\frac{2-\theta\epsilon^2}{3}}\cos\left(\frac{\phi}{3}-\frac{2\pi}{3}\right)\right].$$

Here ϕ is defined by

$$\phi = \arccos\left[-\sqrt{\frac{27(1+\theta\epsilon^2)^2}{4(2-\theta\epsilon^2)^3}}\right]. \tag{A3}$$

Equation (A2) are, to an excellent approximation, equal to

$$\lambda_1 = -\frac{\theta\epsilon}{2}\sqrt{\frac{2}{3}}\cos\left(\frac{1}{3}\arccos\left[-\sqrt{\frac{27}{32}}\right]\right) = -2\,\theta\epsilon,$$

$$\lambda_2 = -\frac{1}{\epsilon}\left[1+2\sqrt{\frac{2}{3}}\cos\left(\frac{1}{3}\arccos\left[-\sqrt{\frac{27}{32}}\right]+\frac{2\pi}{3}\right)\right] = -\frac{3-\sqrt{5}}{2\epsilon},$$

$$\lambda_3 = -\frac{1}{\epsilon}\left[1+2\sqrt{\frac{2}{3}}\cos\left(\frac{1}{3}\arccos\left[-\sqrt{\frac{27}{32}}\right]+\frac{2\pi}{3}\right)\right] = -\frac{3+\sqrt{5}}{2\epsilon}. \tag{A4}$$

We can now write down the solution for $v_1(t)$ by imposing the initial conditions $v_1(0)=V_p$, $\dot{v}_1(0)=-\theta X_1(0)$, $\ddot{v}_1(0)=[\theta X_1(0)/\epsilon]-V_p\theta$, which yields

$$v_1(t) = C_1 e^{\lambda_1 t} + C_2 e^{\lambda_2 t} + C_3 e^{\lambda_3 t}, \tag{A5}$$

where C_1, C_2, C_3 are functions of the eigenvalues and the initial values and given by

$$C_1 = -\frac{\theta - \epsilon V_p - \epsilon\lambda_2\lambda_3 V_p - \epsilon\lambda_2\theta X_1(0) - \epsilon\lambda_3\theta X_1(0)}{\epsilon(\lambda_1-\lambda_2)(\lambda_1-\lambda_3)},$$

$$C_2 = -\frac{-\theta + \epsilon V_p - \epsilon\lambda_1\lambda_3 V_p + \epsilon\lambda_1\theta X_1(0) + \epsilon\lambda_3\theta X_1(0)}{\epsilon(\lambda_1-\lambda_2)(\lambda_2-\lambda_3)},$$

$$C_3 = -\frac{-\theta - \epsilon V_p - \epsilon\lambda_1\lambda_2 V_p - \epsilon\lambda_1\theta X_1(0) - \epsilon\lambda_2\theta X_1(0)}{\epsilon(\lambda_1\lambda_2-\lambda_1\lambda_3-\lambda_2\lambda_3+\lambda_3^2)}.$$

One can easily see that C_1 is of the order of V_p, up to an order ϵ correction, so that $v_2(t)-v_1(t)$ is almost equal to $V_p-v_2(t)$, which shows that the shear rate is homogeneous throughout the flow. The velocity of the first layer slows down to zero exponentially with a typical relaxation rate of $2\,\theta\epsilon$. The second layer is slowed down at the same rate to $V_p/2$,

$$v_2(t) = \frac{V_p}{2}[1+e^{-(2/\epsilon)t}] + C_1\left[\frac{e^{\lambda_1 t}-e^{-(2/\epsilon)t}}{2+\lambda_1\epsilon}\right] + C_2\left[\frac{e^{\lambda_2 t}-e^{-(2/\epsilon)t}}{2+\lambda_2\epsilon}\right] + C_3\left[\frac{e^{\lambda_3 t}-e^{-(2/\epsilon)t}}{2+\lambda_3\epsilon}\right]. \tag{A6}$$

The important convective relaxation time τ_c is given by

$$\tau_c = \frac{1}{2\,\theta\epsilon} = \frac{\eta_0\sqrt{N_e}b}{6k_BT\tau_1\nu} = \frac{\eta_0\sqrt{N_e}}{2b\zeta_1\nu}. \tag{A7}$$

The case $\theta=0$ is simplest since then Eqs. (16) reduce to

$$\epsilon\dot{v}_1 + v_1 = v_2,$$

$$\epsilon\dot{v}_2 + 2v_2 = v_3 + v_1. \tag{A8}$$

Solving for v_1 gives the following expression for $v_1(t)$,

$$v_1(t) = V_p e^{-t/\epsilon} + \frac{e^{-t/\epsilon}}{\epsilon}\int_0^t e^{t'/\epsilon} v_2(t')\,dt'. \tag{A9}$$

When Eq. (A9) is substituted in the evolution equation for v_2, we obtain after differentiating one more time the differential equation for $v_2(t)$,

$$\epsilon\ddot{v}_2 + 3\dot{v}_2 + \frac{v_2}{\epsilon} = \frac{V_p}{\epsilon}, \tag{A10}$$

which is readily solved and gives

$$v_2(t) = V_p + A\exp\left[-\frac{3+\sqrt{5}}{2\epsilon}t\right] + B\exp\left[-\frac{3-\sqrt{5}}{2\epsilon}t\right]. \tag{A11}$$

The coefficients A and B are determined by V_p and the value of the velocity in the first and second layer just before θ becomes zero, $v_1(0)$ and $v_2(0)$, respectively, as follows:

$$A = \frac{v_2(0)(1+\sqrt{5}) + V_p(1-\sqrt{5}) - 2v_1(0)}{2\sqrt{5}},$$

$$B = \frac{v_2(0)(-1+\sqrt{5}) - V_p(1+\sqrt{5}) + 2v_1(0)}{2\sqrt{5}}.$$

For v_1 we have a similar expression as for v_2,

$$v_1(t) = V_p + \left[\frac{2A}{1+\sqrt{5}} - \frac{2B}{-1+\sqrt{5}}\right]\exp\left[-\frac{t}{\epsilon}\right] - \frac{2A}{1+\sqrt{5}} \times \exp\left[-\frac{3+\sqrt{5}}{2\epsilon}t\right] + \frac{2B}{-1+\sqrt{5}}\exp\left[-\frac{3-\sqrt{5}}{2\epsilon}t\right]. \tag{A12}$$

Equations (A11) and (A12) show that the velocity profile jumps, almost instantaneously, back to the initial plug profile.

[1] M. Sun and C. Ebner, Phys. Rev. Lett. **69**, 3491 (1992).
[2] M. Mooney, J. Rheol. **2**, 210 (1931).
[3] P.G. de Gennes, C. R. Seances Acad. Sci., Ser. B **288**, 219 (1979).
[4] F. Brochard and P.G. de Gennes, Langmuir **8**, 3033 (1992).
[5] F. Brochard-Wyart, C. Gay, and P.G. de Gennes, Macromolecules **29**, 377 (1996).
[6] A. Adjari, F. Brochard-Wyart, P.G. de Gennes, L. Leibler, J.L. Viovy, and M. Rubinstein, Physica A **204**, 17 (1994).
[7] K.B. Migler, H. Hervet, and L. Léger, Phys. Rev. Lett. **70**, 287 (1993).
[8] K.B. Migler, G. Massey, H. Hervet, and L. Léger, J. Phys.: Condens. Matter **6**, A301-304 (1994).
[9] L. Léger, H. Hervet, G. Massey, and E. Durliat, J. Phys.: Condens. Matter **9**, 7719 (1997).
[10] J.D. Shore, D. Ronis, L. Piché, and M. Grant, Phys. Rev. E **55**, 2976 (1997).
[11] J.D. Shore, D. Ronis, L. Piché, and M. Grant, Phys. Rev. Lett. **77**, 655 (1996).
[12] Y.M. Joshi, A.K. Lele, and R.A. Mashelkar, Macromolecules **34**, 3412 (2001).
[13] Y.M. Joshi and A.K. Lele, J. Rheol. **46**, 427 (2002).
[14] D.W. Mead, R.G. Larson, and M. Doi, Macromolecules **31**, 7895 (1998).
[15] C.C. Hua and J.D. Schieber, J. Chem. Phys. **109**, 10 018 (1998); C.C. Hua, J.D. Schieber, and D.C. Venerus, *ibid.* **109**, 10 028 (1998).
[16] G.C. Georgiou, Rheol. Acta **35**, 19 (1996).
[17] P.P. Drda and S.Q. Wang, Phys. Rev. Lett. **75**, 2698 (1995).
[18] Y. Inn and S.Q. Wang, Phys. Rev. Lett. **76**, 467 (1996).
[19] M.M. Denn, Annu. Rev. Fluid Mech. **22**, 13 (1990).
[20] M.M Denn, Annu. Rev. Fluid Mech. **33**, 265 (2001).
[21] S.G. Hatzikiriakos and J.M. Dealy, J. Rheol. **36**, 845 (1992).
[22] M. Doi and S.F. Edwards, *The Theory of Polymer Dynamics* (Oxford Science Publications, New York, 1986).
[23] D.S. Pearson and E. Helfland, Macromolecules **17**, 888 (1984).
[24] R.C. Ball and T.C.B. McLeish, Macromolecules **22**, 1911 (1989).
[25] A.L. Yarin and M.D. Graham, J. Rheol. **42**, 1491 (1998).
[26] J. Den Doelder, Ph.D. thesis, TU, Eindhoven, 2000.